

Research paper

Anomalous positive pyrite sulfur isotope in lacustrine black shale of the Yanchang Formation, Ordos Basin: Triggered by paleoredox chemistry changes



Guo Chen ^{a,*}, Xiangchun Chang ^a, Wenzhe Gang ^b, Ning Wang ^b, Pengfei Zhang ^a, Qingyun Cao ^c, Jianbin Xu ^d

^a College of Earth Science and Engineering, Shandong University of Science and Technology, Qingdao, 266590, China

^b College of Geosciences, China University of Petroleum, Beijing, 102249, China

^c No.2 Gas Production Plant of PetroChina Changqing Oilfield Company, Yulin, 719000, China

^d Exploration and Development Research Institute of PetroChina Liaohe Oilfield Company, Panjin, 124010, China

ARTICLE INFO

Keywords:

Pyrite
Sulfur isotope
Paleoredox chemical condition
The chang 7 unit

ABSTRACT

The pyrite sulfur isotope in the black shale of the Chang 7 unit are anomalous positive compared with those of the current paradigm, in which the value of pyrite sulfur isotopes should be negative due to sulfur isotopic fractionation through bacterial sulfate reduction (BSR). A series of geological and geochemical analysis ($\text{Fe}_\text{T}/\text{Al}$ and $\delta^{34}\text{S}_{\text{py}}$, average of 0.51 and 6.5‰, respectively) are carried out to confirm that sulfur speciation is derived from sulfate in watermass rather than hydrothermal fluids, and the $\delta^{34}\text{S}_{\text{py}}$ values are effective records of the original sedimentary environment. Integrated geochemical data including redox sensitive elements (RSE) ratios, ratio of organic carbon to phosphorus ($\text{C}_{\text{org}}/\text{P}$, molar, average of 85.4), organic sulfur to carbon (organic S:C, average of 10.47%) and pyrite frambooid size distribution (range in 9.7–16.6 μm), are represented to reconstruct the paleoredox chemical conditions during the deposition of the Chang 7 unit black shale. The results suggest that the paleoredox chemical conditions of the middle and lower subunits (the Ch 7₂ and Ch 7₃ subunits) were dominated by suboxic environments with intermittent anoxic environments and that changed to oxic with intermittent suboxic environments in the upper subunit (the Ch 7₁ subunit). Based on the analysis of sulfur isotope fractionation during the sulfur cycle, the paleoredox chemical conditions are confirmed to be the trigger for the anomalous sulfur isotopic compositions. The limited sulfate in watermass and overlying fine-grained sediments resulted in a relatively closed system for BSR, where limited sulfur isotope fractionation lead to the formation of heavy pyrite. Subsequently, due to the dissolved oxygen penetrated into the sediment, the reactivation of anaerobic oxidants resulted in reoxidation of hydrogen sulfide derived from BSR, then to “heavier” pyrite via Rayleigh-type distillation in the Ch 7₁ subunit.

1. Introduction

Sulfur is a widespread element in nature that plays an important role in many natural processes, and knowledge of the sulfur isotopic composition can enhance the understanding of various geological processes in geological history (Lowenstein et al., 2005; Zerkle et al., 2010; Johnston, 2011; Wang et al., 2019; Pang et al., 2020). Particularly in a sedimentary basin, sulfate is an essential joint linking the carbon, sulfur and iron cycles through geochemical processes such as bacterial sulfate reduction (BSR), iron sulfide formation, and organic matter sulfuration

(Anderson and Pratt, 1995; Canfield, 2001; Habicht and Canfield, 2001; Hurtgen et al., 2002). Bacterial sulfate reduction (BSR) is an anaerobic process occurring in anoxic conditions with abundant organic matter as a reductant that couples sulfur with carbon and iron through the reduction of sulfate, and results in a depletion of ^{34}S in sulfide products (such as pyrite) relative to coeval carbonate-associated sulfate if no obvious alteration occurs in burial process (Berner and Raiswell, 1983; Kleeberg, 1997; Sim et al., 2011). For example, the sulfur isotope of pyrite and carbonate-associated sulfate (represent as $\delta^{34}\text{S}_{\text{py}}$ and $\delta^{34}\text{S}_{\text{CAS}}$, respectively) across the F–F (Frasnian-Famennian) boundary in South

* Corresponding author.

E-mail address: cupchenguo@outlook.com (G. Chen).

China vary from -18.5‰ to 26.7‰ and 9.7‰ – 35.4‰ , respectively (Chen et al., 2013); the $\delta^{34}\text{S}_{\text{py}}$ and $\delta^{34}\text{S}_{\text{CAS}}$ across the Permian-Triassic boundary in South China vary from -39.7‰ to 9.5‰ and 17.0‰ – 27.5‰ , respectively (Shen et al., 2016; Luo et al., 2010). Since significant cycles between sulfate and sulfide are accompanied by organic/inorganic carbon and iron cycles, the sulfur isotopic composition can be used to reconstruct fluctuations in the sedimentary environment (Yan et al., 2012; Wei et al., 2016; Liu et al., 2019a, b).

However, “heavy” pyrite with ^{34}S enrichment has also been reported worldwide, such as that in the Qingshankou Formation (Huang et al., 2013) and the Chang 7 unit (Zhang et al., 2010) in China, the Random Formation in Canada (Strauss et al., 1992), and the Lublin Formation in Poland (Bottomley et al., 1992). Previous studies have proposed several mechanisms to explain the peculiar “heavy” pyrite sulfur isotope: 1) a low sulfate concentration in watermass results in very limited sulfur fractionation in the closed system (Canfield, 2001; Huang et al., 2013); 2) hydrogen sulfide derived from BSR is reoxidized leading to the “heavy” pyrite sulfur isotope (Canfield, 2001; Ries et al., 2009); 3) a

mixture of a small amount of isotopically light syngenetic pyrite (precipitated in the water column) with more isotopically heavy diagenetic pyrite (formed via in situ BSR) (Algeo et al., 2008). However, the diagenetic organic sulfur compounds (OSCs) from organic matter sulfuration are rarely mentioned in the discussion of the sulfur cycle as the second most important sulfur speciation in the sediments after pyrite (Anderson and Pratt, 1995; Werne et al., 2004). The Chang 7 unit in the Ordos Basin has characteristics of anomalous positive pyrite sulfur isotope, which has been considered to be the result of hydrothermal fluids (Zhang et al., 2010). Recent geochemical researches suggest that the anomalous sulfur isotopic composition in marine sediments could be relevant to paleoredox chemical condition (Canfield, 2001; Ries et al., 2009), but the relevant research focus on the effect of redox condition on pyrite sulfur isotope of lacustrine sediment is still lacking. In addition, the vast research focused on the sedimentary environment during the deposition of the Chang 7 unit is still confusing due to the effects of vast volcanic and hydrothermal products on redox sensitive elements (RSEs) and extract biomarkers, petromineralogy characteristics, etc. (Zhang

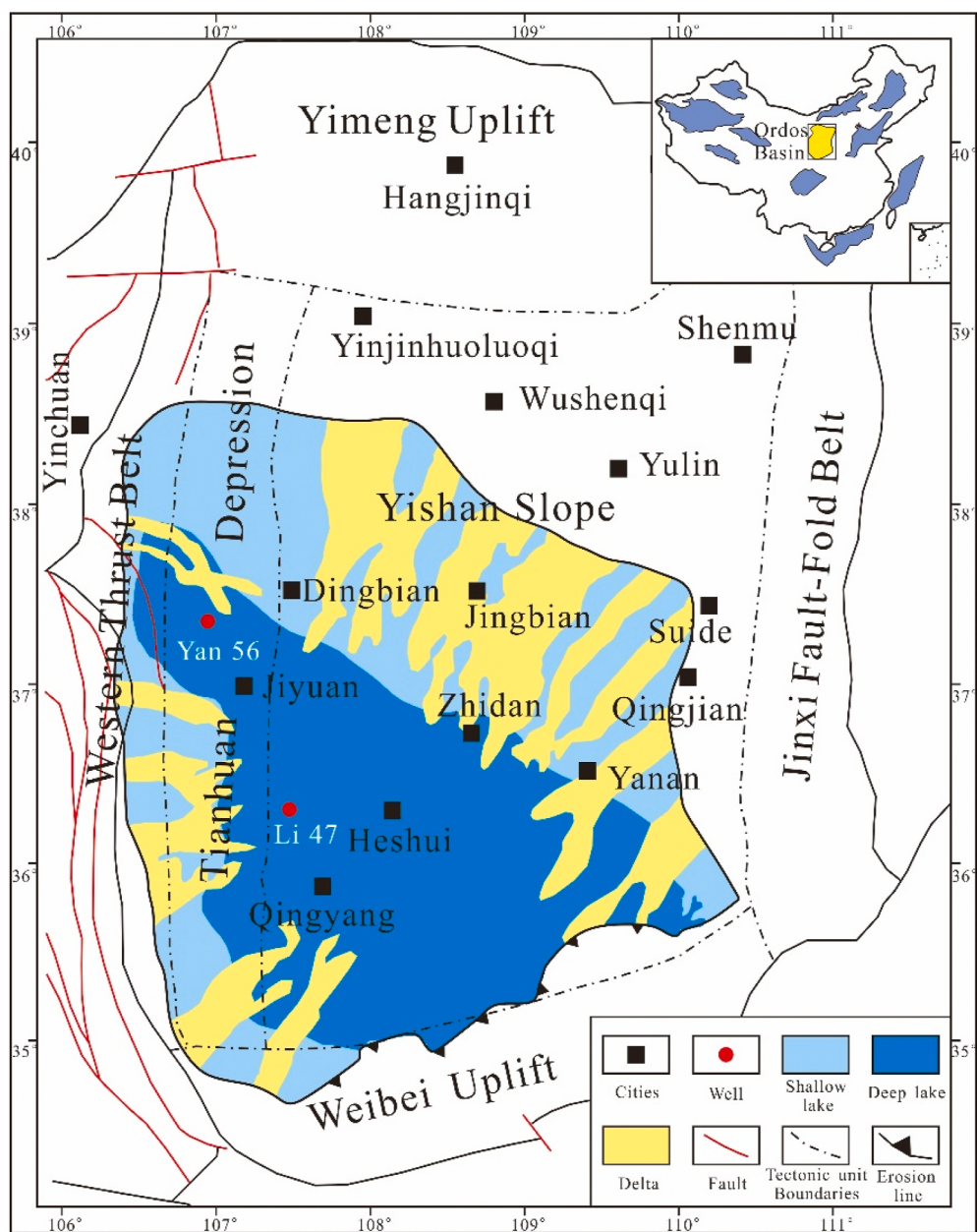


Fig. 1. Map showing the location of the Ordos Basin, tectonic units, sedimentary facies, and the sample well (modified from Chen et al., 2019a).

et al., 2017; Yuan et al., 2017; Chen et al., 2019b; Li et al., 2019; Zhang et al., 2020).

In this study, the pyrite sulfur isotope ($\delta^{34}\text{S}_{\text{py}}$), organic carbon isotope ($\delta^{13}\text{C}_{\text{oc}}$) and total iron content (Fe_T) of the continuous drillcore

samples from the Chang 7 unit were presented to discuss the sulfur derivation of pyrite in the black shale. In addition, integrated geochemical data were utilized to reconstruct the changes in the paleoredox chemical conditions, including the RSE, ratio of organic carbon

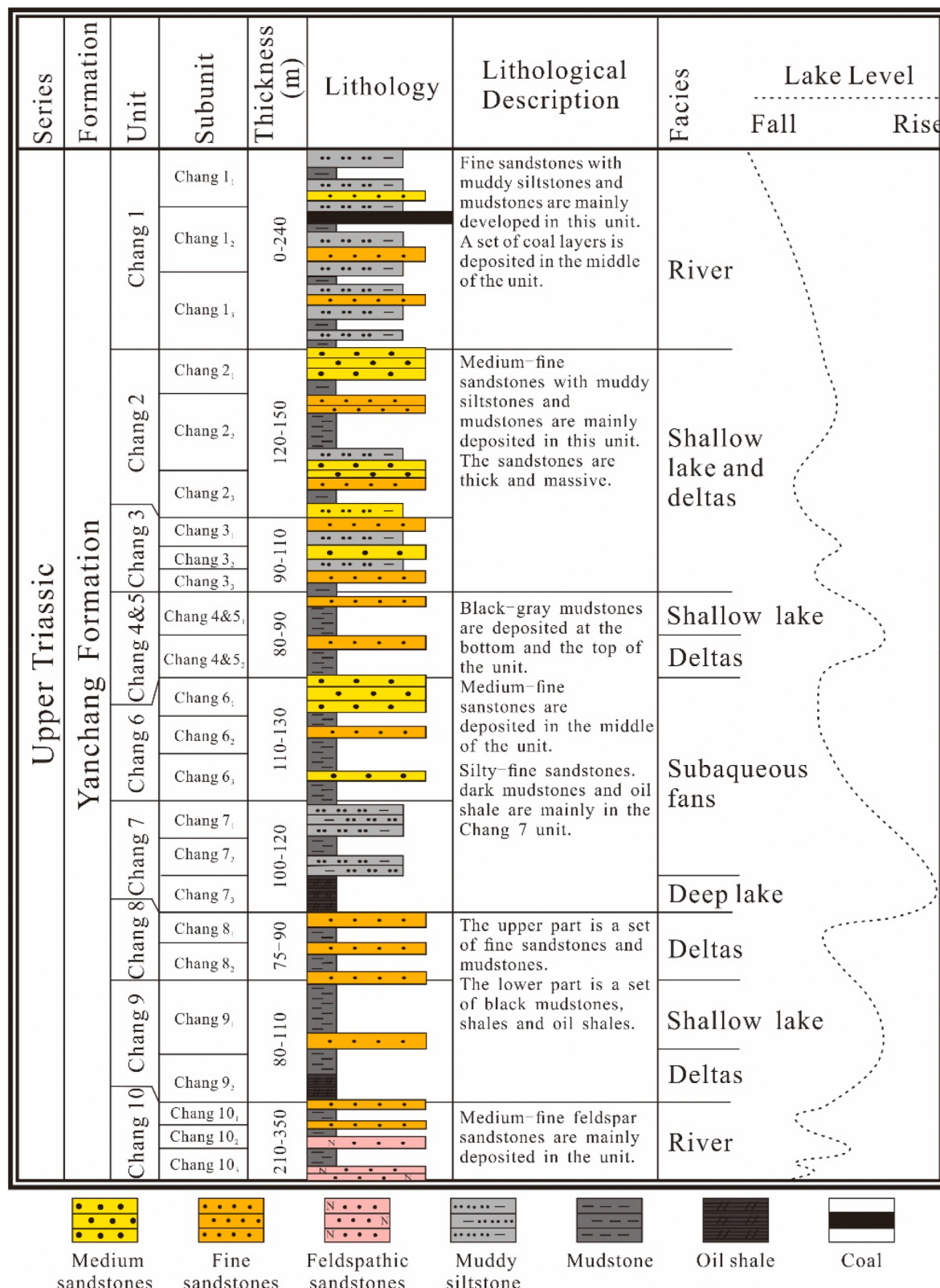


Fig. 2. Triassic stratigraphy of the Yanchang Formation, showing the Upper Triassic strata, the lithology and thickness of each unit, the sedimentary facies, and lake-level fluctuations (modified from Chen et al., 2019a).

to phosphorus, organic sulfur to carbon and pyrite framboid size distribution. Finally, the variations of the pyrite sulfur isotope and paleoredox chemical conditions were combined to explore the formation mechanism of the heavy pyrite formation during the deposition of the Chang 7 unit black shale.

2. Geologic setting

The Ordos Basin is the second-largest petrolierous basin in China covering more than 250,000 km² (Yang et al., 2010). The Ordos Basin consists of six tectonic units, including the Yimeng Uplift, the Western Thrust Belt, the Tianhuan Depression, the Yishan Slope, the Weibei Uplift, and the Jinxi Fault-Fold Belt based on tectonic characteristics (Yang, 2002, Fig. 1). Before the Late Permian period, the Ordos Basin was a part of the North China Block and was characterized by a passive continental basin developed on the Paleoproterozoic basement (Zhang et al., 2008; Qiu et al., 2014). Subsequently, the Ordos Basin went through an essential transformation from shallow marine facies to continental lacustrine facies (Zhu et al., 2008; Zou et al., 2010; Qiu et al., 2014). By the Late Triassic, the North China Block was impacted on the Yangtze Block, and subsequently sutured to an entire continent with the uplift of the Qinling Mountains (Yang, 2002). Meanwhile, the intense tectonic movement led to frequent volcanic activity and maximum expansion of the lacustrine basin during the Late Triassic (Yang, 2002; Qiu et al., 2014). Based on the tectonic setting, the fluvial to lacustrine sediments with laminated volcanic ash intervals were widely distributed in the Ordos Basin during the Late Triassic to Cretaceous with a thickness of approximately 4000 m (Zhu et al., 2013; Qiu et al., 2014). In particular, the Yanchang Formation recorded that the complete evolution stage of the lacustrine sediments can be divided into 10 units namely the Chang 1 unit to the Chang 10 unit from top to bottom, based on rhythmic lithological alternations (Guo et al., 2014; Qiu et al., 2015, Fig. 2). The target stratum in this study, the Chang 7 unit, developed in the middle-lower part of the Yanchang Formation when the Ordos lacustrine basin expanded to its maximum area, which led to the deposition of organic-rich shale (Yuan et al., 2017; Chen et al., 2019b). The lithology of the Chang 7 unit deposits mainly changes from black shale to mudstone and then to siltstone with the shrinking of the lake basin. Vast laminated volcanic ash intervals are mixed in the sediments, especially in the lower part of the Chang 7 unit (Zhu et al., 2013). The Chang 7 unit black shale has been considered to be the main hydrocarbon source rock for the Mesozoic petroleum system and is mainly characterized by high organic matter abundance, favorable organic matter type and appropriate organic matter maturity for hydrocarbon generation (Zhang et al., 2015 2017; Liu et al., 2018; Chen et al., 2019a).

The study area, the Yanchi-Dingbian area, is located in the conjunction of the Tianhuan Depression and the Western Thrust Belt with an area of 4000 km² (Fig. 1). Since the study area is situated in the north periphery of the lacustrine basin, which is far from the zone of volcanic activity, the influence of volcanic and hydrothermal activities on the sediments of the Chang 7 unit is limited, which is beneficial for the study of the fluctuations in the sedimentary environment.

3. Sampling and methods

Numerous sedimentary environment analyses were carried out on a total of 39 continuous drillcore samples from the Yan 56 well, including analyses of the total organic carbon content (TOC), total sulfur content (TS), pyrite sulfur isotopes ($\delta^{34}\text{S}_{\text{py}}$), organic carbon ($\delta^{13}\text{C}_{\text{oc}}$) isotopes, trace element content and iron speciation content. Before analysis, approximately 3–5 mm slice were incised from the surface of rock samples to reduce the influence of sample oxidation.

All the selected samples were crushed to powder, and then sieved with an 80-mesh sieve. Hydrogen chloride (HCl) at 10% (%) was mixed into all the powdered samples to eliminate the effect of inorganic carbon. Then, distilled water was used to remove the traces of HCl. Finally,

a Leco CS-230 analyzer was used to perform the TOC and TS analyses on all the samples. For detailed descriptions, refer to Chen et al. (2019c).

Twenty samples were selected to cut into small pieces to eliminate euhedral pyrite and aggregates. The pyrite sulfur isotopes were analyzed using the chromium reduction method (Canfield et al., 1986). The pyrite sulfur was extracted on the basis of Chu et al. (1993). Moderate powder samples were blended with 4.8 mol/L HCl for longer than 2 h at 75 °C to eliminate acid volatile sulfide (AVS). The residual solution was blended with bromide water until the solution became achromatic. Then, 15 ml of 10% barium chloride solution was added to the reaction mixture for approximately 1 h, and the reaction mixture was set aside for approximately 12 h. The residue was leached with deionized water and then treated with 100 ml chromium chloride solution and high concentration HCl heated at 120 °C for 1 h. The released hydrogen sulfide gas was bubbled into a mixed solution of 2% silver nitrate solution and 10% ammonium hydroxide, and then, the solution was used to filter the silver sulfide (Ag₂S) precipitate for $\delta^{34}\text{S}_{\text{py}}$ analysis. Subsequently, the Ag₂S precipitated from the pyrite was mixed with cuprous oxide and combusted to generate sulfur dioxide (SO₂) for sulfur isotope analysis, performed on a Flash 2000 EA-Delta V Plus IRMS at the Analytical Laboratory of the Beijing Research Institute of Uranium Geology (ALBRIUG). The analytical precision of the device is limited to $\pm 0.2\%$ for $\delta^{34}\text{S}$, and the $\delta^{34}\text{S}$ was shown as per mil (‰) relative to the Vienna Canyon Diablo Troilite (VCDT) standard and was calibrated using the international standards: IAEA-S-1 ($\delta^{34}\text{S}$: −0.30‰), IAEA-S-2 ($\delta^{34}\text{S}$: 22.64‰) and IAEA-S-3 ($\delta^{34}\text{S}$: −32.06‰).

After eliminating the inorganic carbon by mixing the sample with 10% HCl, the carbon isotope analysis of the organic carbon ($\delta^{13}\text{C}_{\text{oc}}$) was carried out by a Flash HT EA-MAT 253 IRMS at the SKLPRP, China University of Petroleum (Beijing). The analytical precision is limited to $\pm 0.1\%$ for $\delta^{13}\text{C}_{\text{oc}}$. All the $\delta^{13}\text{C}_{\text{oc}}$ data were reported as per mil (‰) relative to the Vienna Pee Dee belemnite (VPDB) standard and were calibrated using the international standards: GBW04408: $\delta^{13}\text{C}$: −36.9‰, IAEA-600-Caffeine: $\delta^{13}\text{C}$: −27.8‰, USGS 24 Graphite: $\delta^{13}\text{C}$: −16.1‰ and internal laboratory standard: $\delta^{13}\text{C}$: −27.0‰.

Major oxides and trace elements of all selected samples were analyzed at ALBRIUG with X-ray fluorescence and Inductively coupled plasma-mass spectrometry (ICP-MS), respectively. An agate mortar was used to grind rock sample until sample powder passed through 200-mesh sieve. Major oxides (include SiO₂, Al₂O₃, Fe₂O₃, MgO, CaO, Na₂O, K₂O, MnO, TiO₂ and P₂O₅) analysis were carried on an Axiosm AX XRF spectrometer. For trace elements analysis, all samples were dissolved using HF (30%) and HNO₃ (68%) at 190 °C for 24 h. After evaporating excess solvent at 130 °C for 3 h, the samples were re-dissolved in 2 ml of 6 mol/L HNO₃ in capped Teflon bombs at 150 °C for 48 h. Then, the trace elements analysis were performed on an Element XR ICP-MS based on the Chinese National Standard GB/T 14506.30–2010. The detection limit for trace elements was 0.1×10^{-12} to 9×10^{-12} .

The highly reactive iron speciation includes Fe_{py}, Fe_{carb}, Fe_{ox} and Fe_{mag}. The Fe_{py} extract procedure was based on Canfield et al. (1986), and the other reactive iron speciation (Fe_{carb}, Fe_{ox} and Fe_{mag}) was measured according to following extraction procedure (Poulton and Canfield, 2005). A quadrupole ICP-MS was used to stoichiometrically analyze the iron contents of all the iron speciation extractions at the State Key Laboratory of Biogeology and Environmental Geology, China University of Geosciences (Wuhan).

4. Results

The stratigraphic variations of the TOC, TS, $\delta^{34}\text{S}_{\text{py}}$, $\delta^{13}\text{C}_{\text{oc}}$, major oxides(P₂O₅, Al₂O₃, Fe₂O₃ and MnO₂), RSE (barium, vanadium, chromium, uranium, thorium, copper and zinc) and iron speciation (Fe_T, Fe_{py}, Fe_{carb}, Fe_{ox} and Fe_{mag}) contents, and the calculated parameters organic S:C, Fe_T/Al, sulfur speciation (S_{py}, S_{barite} and S_{om}), V/Cr, U/Th, Cu/Zn, C_{org}:P and Fe_X/Fe_T of the Chang 7 unit are shown in Table S1 and

Figs. 3&4.

Nearly all the samples from the Chang 7 unit have high TOCs that are in the range of 0.68–8.72% with an average of 4.71% (Fig. 3), which indicates that the Chang 7 unit sediments are excellent hydrocarbon source rocks (Dembicki, 2009). Through the stratigraphic section, the TOC fluctuates with the lithology, and the Ch 7₂ and Ch 7₃ subunits show higher TOC than that of the Ch 7₁ subunit. The TS contents of all the samples vary from 0.07% to 5.17% with the TOC, with an average of 1.35 (Fig. 3).

The pyrite sulfur isotope ($\delta^{34}\text{S}_{\text{py}}$) values across the Chang 7 unit are presented in Fig. 3 and Table S1. The $\delta^{34}\text{S}_{\text{py}}$ values are in the range of 3.4‰–12.0‰ with an average of 6.5‰, and $\delta^{34}\text{S}_{\text{py}}$ show relative low values in the Ch 7₂ and Ch 7₃ subunits, and then shift to high values in the Ch 7₁ subunit (Fig. 3). The carbon isotope values of the organic matter ($\delta^{13}\text{C}_{\text{OC}}$) vary from –30.1‰ to –28.9‰ with an average of –29.5‰, which represents a narrow distribution range (Fig. 3; Table S1).

The total iron-compound contents of all the samples in the studied interval exceed 0.5% and vary from 2.96% to 12.80% with an average of 6.48%, and the Fe_T contents gradually increase from the bottom to top (Fig. 4; Table S1). The Al₂O₃, P₂O₅ and MnO₂ contents are in the range of 14.72%–21.05%, 0.19%–3.35% and 0.03%–0.40%, respectively (Table S1). In addition, the iron derivation parameter Fe_T/Al and paleoredox chemical parameter C_{org}:P (molar) are in the range of 0.22–1.06 (average of 0.51) and 11.9–162.0 (average of 85.4) (Fig. 4; Table S1). The trace elements concentrations including Ba, V, Cr, U, Th, Cu and Zn are shown in Table S1, and the derived redox sensitive elements (RSE) ratio such as V/Cr, U/Th and Cu/Zn through whole section are in the range of 0.79–2.22 (average of 1.39), 0.19–3.10 (average of 0.59) and 0.25–1.14 (average of 0.62), respectively (Fig. 4; Table S1).

Based on the iron speciation analysis, all the highly reactive iron speciation (Fe_{HR}) can be quantified, including Fe_{py}, Fe_{carb}, Fe_{ox} and Fe_{mag}. The relative contents of Fe_{ox} and Fe_{mag} are mainly lower than 5%,

and reductive iron (Fe_{py}, Fe_{carb}) is present at contents relatively higher than those of Fe_{ox} and Fe_{mag}, with relative content greater than 10% or even greater than 35% (Fig. 4; Table S1).

Pyrite, barite and organically bound sulfur are major sulfur species in sediments. Assuming that all Ba is present as barite, the organic sulfur can be present as sulfur from barite and pyrite subtracted from total sulfur (TS-S_{py}-S_{barite}) (Cai et al., 2015). The sulfur contents from pyrite and barite are in the range of 0.02%–2.10% and 0.01%–0.03%, respectively. Thus, the calculated total organic sulfur (TOS) range from 0 to 3.05% with an average of 0.86% (Fig. 3; Table S1).

5. Discussion

5.1. Derivation of sulfur in the Chang 7 unit black shale

The sulfur isotopic composition of the Chang 7 unit black shale is characterized by anomalous high $\delta^{34}\text{S}_{\text{py}}$ values compared with those of other study areas. Because the sulfur isotopic composition is the main object of this study, it is important to discuss whether the $\delta^{34}\text{S}_{\text{py}}$ have suffered contamination and diagenetic influences. For example, pyrite is often formed in large euhedral pyrite with diagenetic growth or overgrowth (Wilkin et al., 1996; Shen et al., 2016). But the thin section shows that the pyrite is mainly represented as sporadic frambooids without obvious diagenetic growth or overgrowth (Zhang et al., 2010; Chen et al., 2019b). The anomalous positive $\delta^{34}\text{S}_{\text{py}}$ values are ubiquitous in the Chang 7 unit (Zhang et al., 2009&2010, Fig. 3), which indicates that the positive $\delta^{34}\text{S}_{\text{py}}$ values are not a result of the sample preparation or analysis. In addition, the weak, but positive correlation between $\delta^{13}\text{C}_{\text{OC}}$ and TOC suggests that the $\delta^{13}\text{C}_{\text{OC}}$ variations were not caused by thermal alterations during diagenesis (Fig. 5A). Interestingly, there is an obviously negative relationship between $\delta^{34}\text{S}_{\text{py}}$ and $\delta^{13}\text{C}_{\text{OC}}$ for the Ch 7₁ subunit, but such a relationship does not occur for the Ch 7₁ and Ch 7₂ subunits (Fig. 5B), which indicate that the coupling of $\delta^{34}\text{S}_{\text{py}}$ and $\delta^{13}\text{C}_{\text{OC}}$

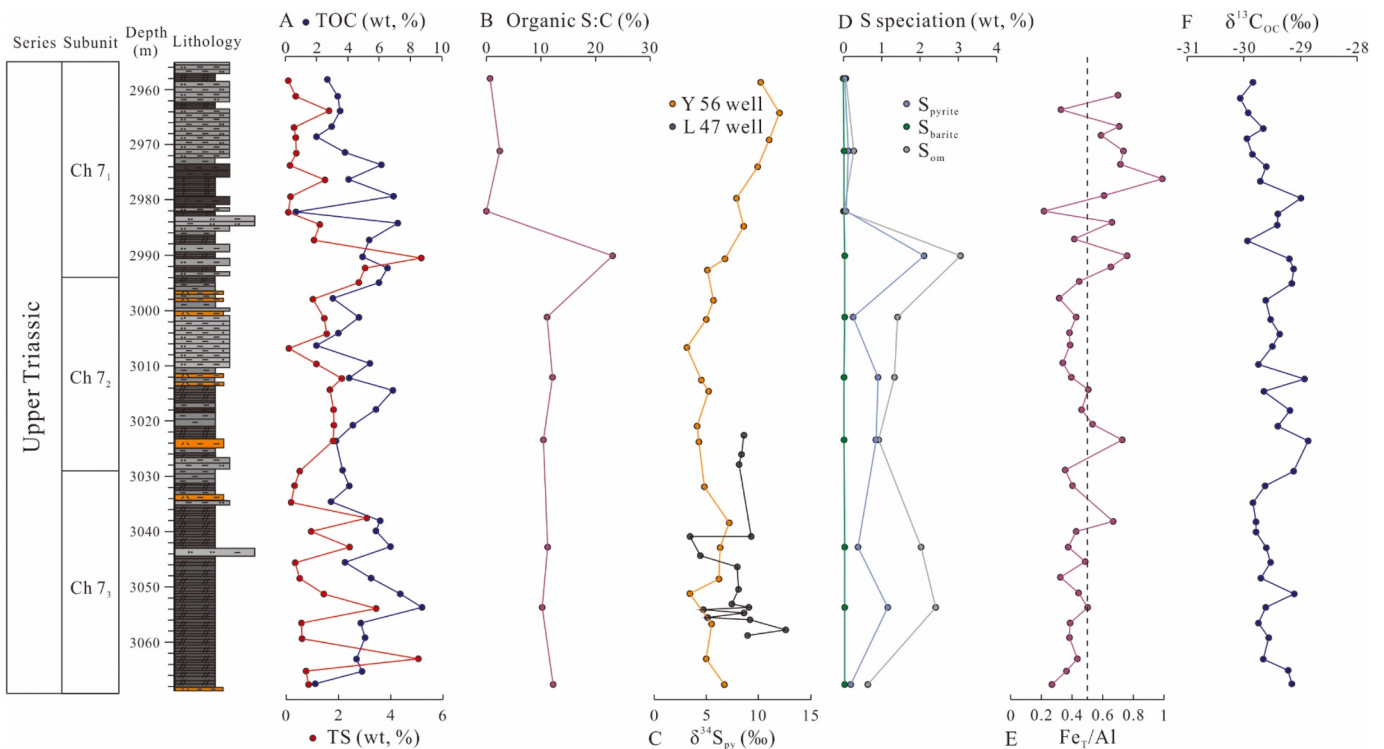


Fig. 3. Geochemical profiles of the Chang 7 unit black shale: (A) total organic carbon content (TOC) and total sulfur (TS) of the Chang 7 unit from Y 56 well; (B) organic S:C ratios of the Chang 7 unit from Y 56 well; (C) pyrite sulfur isotopes ($\delta^{34}\text{S}_{\text{py}}$) of the Chang 7 unit from Y 56 well and L 47 well; the $\delta^{34}\text{S}_{\text{py}}$ of the L 47 well is based on Zhang et al. (2010); (D) sulfur speciation (including S_{pyrite}, S_{barite} and S_{om}) content of the Chang 7 unit from Y 56 well; (E) Fe/T/Al ratios of the Chang 7 unit from Y 56 well; (F) organic matter carbon isotopes ($\delta^{13}\text{C}_{\text{OC}}$) of the Chang 7 unit from Y 56 well. ratio of organic carbon to phosphorus (C_{org}:P) of the Y 56 well.

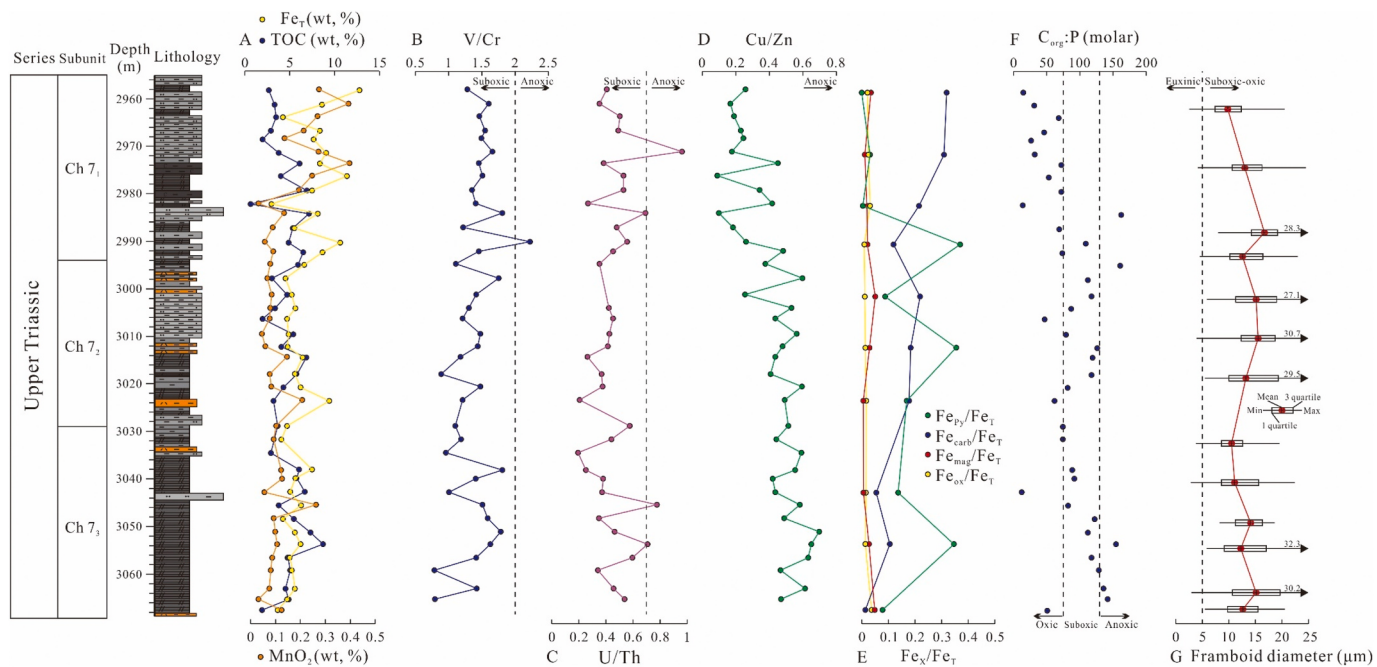


Fig. 4. Geochemical profiles of the Chang 7 unit black shale: (A) total organic carbon content (TOC), total iron content (Fe_T) and manganese dioxide content (MnO_2) of the Chang 7 unit from Y56 well; (B) ratio of vanadium to chromium (V/Cr) of the Chang 7 unit from Y56 well; (C) ratio of uranium to thorium (U/Th) of the Chang 7 unit from Y56 well; (D) ratio of copper to zinc (Cu/Zn) of the Chang 7 unit from Y56 well; (E) iron speciation relative content of the Chang 7 unit from Y56 well; (F) ratio of organic carbon to phosphorus ($\text{C}_{\text{org}}:\text{P}$, molar) of the Chang 7 unit from Y56 well; and (G) pyrite framboid size distribution (data from Chen et al., 2019b).

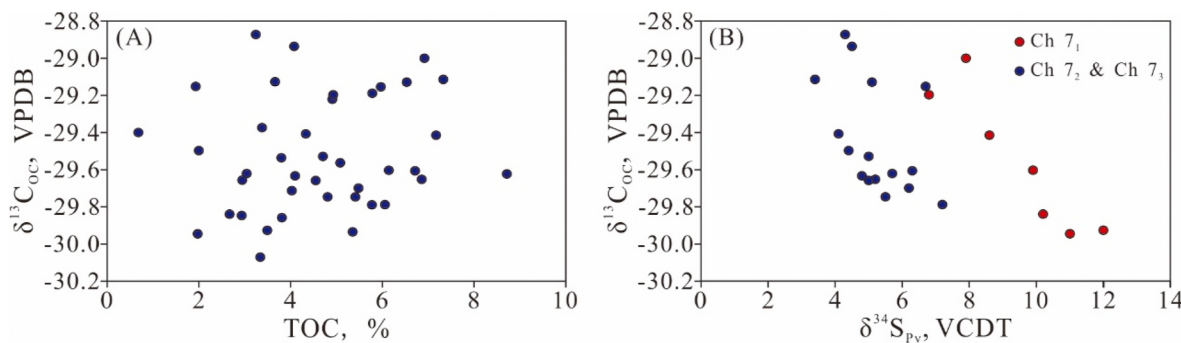


Fig. 5. (A) Cross-plot of $\delta^{13}\text{C}_{\text{oc}}$ values and TOC contents of the Chang 7 unit from Y56 well; (B) cross-plot of $\delta^{13}\text{C}_{\text{oc}}$ values and $\delta^{34}\text{S}_{\text{py}}$ values of the Chang 7 unit from Y56 well.

of the Chang 7 unit can reflect the original sedimentary environment.

Generally, the sulfur derivation of lake water includes the following: 1) dissolved evaporites (with $\delta^{34}\text{S}$ range of 10–30‰) and oxidized pyrite (with $\delta^{34}\text{S}$ range of –40–5‰); 2) atmospheric precipitation and surface-runoff (with $\delta^{34}\text{S}$ range of 3–15‰); 3) volcano and hydrothermal system (with $\delta^{34}\text{S}$ range of –10–15‰); and 4) marine incursion (Canfield, 2001). The BSR activity has been considered to be the most significant sulfur isotopic fractionation of ^{34}S and ^{32}S , leading to a ^{34}S depletion in the hydrogen sulfide and subsequent product compared with the $\delta^{34}\text{S}$ values of coeval sulfate (Kaplan and Rittenberg, 1964; Canfield, 2001). According to the BSR reaction mechanism, abundant organic carbon, sufficient sulfate concentration and a reducing environment are the most appropriate conditions for the crystallization of syngenetic pyrite (Ryu et al., 2006; Nara et al., 2010). Particularly in an open environment where adequate exchange occurs between the sulfate in pore water and overlying watermass, the sulfur isotopic fractionation between pyrite and coeval sulfate is greater than 20‰ (Zaback et al., 1993; Habicht and Canfield, 1997). However, the pyrite sulfur isotope of the Chang 7 unit represents anomalous heavy pyrite in black shale. Previous studies considered that the anomalous sulfur isotopic composition of pyrite may

be caused by lake-bottom hydrothermal activity. An amount of sulfide accompanied by hydrothermal fluids intruded into the watermass, which resulted in the formation of pyrite in the Chang 7 unit black shale. That is, the derivation of pyrite sulfur comes from sulfide in hydrothermal fluids rather than watermass from BSR (Zhang et al., 2010). Two lines of evidence have been proposed to certify this opinion: 1) the $\delta^{34}\text{S}_{\text{py}}$ values are similar to the $\delta^{34}\text{S}$ values of volcanic products ($\delta^{34}\text{S} = 2.2 \pm 0.3\text{\textperthousand}$; Wei and Wang, 1988) derived from mantle sources and 2) a number of mineral assemblages associated with hydrothermal activity, such as siliceous rock, ankerite laminar deposits, and marcasite-brassil-anhydrite symbiosis systems (Zhang et al., 2010&2017). However, the sulfur isotope of sulfide has been considered to be a sedimentary record that is relative not only to the origin of the sulfide but also the sulfate concentration in watermass and redox chemical conditions of bottom water and sedimentary facies (Canfield, 2001). In a low sulfate closed system, due to the insufficient supply of sulfate, ^{32}S -sulfate is consumed rapidly, and to sustain the BSR reaction, ^{34}S -sulfate participates in the reaction (Canfield, 2001). This situation results in the sulfur isotopic fractionation being restricted, and the sulfur isotope of the sulfide is “inherited” from the sulfur isotope of sulfate due

to the complete BSR reaction (Hurtgen et al., 2002; Kah et al., 2004). Because the expansion of hydrothermal activity can increase the concentration of hydrothermal Fe in sediment, resulting in an elevated Fe_T/Al much greater than 0.5, the continental crustal average value (Taylor and McLennan, 1995; Owens et al., 2012). The Fe_T/Al ratios through whole section show an average of 0.51, which is assumed to represent typical siliciclastic/detrital input without hydrothermal input (Fig. 3; Table S1). Interestingly, the higher value of Fe_T/Al in the Ch 7₁ subunit (average of 0.67) than that in the Ch 7₂ and Ch 7₃ subunits (average of 0.45) maybe caused by the reduced BSR intensity, which inhibited sedimentary Fe dissolved in the pore fluids, and transported from the sediment to watermass (Lyons and Severmann, 2006; Severmann et al., 2010). Furthermore, the sulfate concentration in watermass is consecutively decreased and deposited ^{32}S as sulfides in priority from source to sink (Huang et al., 2013). However, the average $\delta^{34}\text{S}_{\text{py}}$ value of the Chang 7 unit in the Y56 well is lower than that in the L47 well, which is closer to volcanic and hydrothermal activity area (joint of the Yishan Slope and the Weihei Uplift) (Fig. 1), indicating that the sulfur derivation is not from hydrothermal fluids. As a whole, the derivation of sulfur in the Chang 7 unit black shale is from sulfate in watermass mainly derived from atmospheric precipitation/surface-runoff rather than a hydrothermal system, and the pyrite sulfur isotope of the Chang 7 unit black shale could be a record of depositional environmental change.

5.2. Paleoredox chemistry changes

Due to the variational chemical properties of RSE under different redox condition, the RSE ratios can be used as effective geochemical parameters to evaluate the paleoredox conditions (Jones and Manning, 1994). For example, vanadium (V) usually occurs as V^{5+} in an oxic condition, while in the form of V^{3+} or V^{4+} in a reducing condition (Jones and Manning, 1994), where V^{3+} or V^{4+} could be transferred to sediments by absorption or the formation of organometallic ligands (Morford and Emerson, 1999). In addition, chromium (Cr) occurs as the oxidized oxyanion chromate (CrO_4^{2-}) in an oxic condition, which results in Cr transfer to watermass column (Canfield et al., 1986). Thus, the paleoredox condition changes from oxic to anoxic gradually with increasing V/Cr ratios, and V/Cr ratio in the range of 1.2–2.0 indicate a suboxic condition (Rimmer, 2004). Furthermore, uranium (U) occurring in watermass is mainly in the form of $[\text{UO}_2(\text{CO}_3)_3]^{4-}$, which was stable in watermass rather than be absorbed to Fe–Mn metal particle under oxic condition (Anderson et al., 1989). In the reducing condition, U could transfer to sediments in the form of UO_2 reduced from $[\text{UO}_2(\text{CO}_3)_3]^{4-}$ (Anderson et al., 1989). Thorium (Th) is relatively immobile in the natural environment and is concentrated in terrestrial detrital fraction. Hence, the U/Th ratio can serve as an effective paleoredox condition indicator, and U/Th ratio in 0.3–0.7 suggest a suboxic condition. Likewise, Cu and Zn have a semblable chemical character as U and Th, and the increasing Cu/Zn ratio indicate a more reducing condition. Based on the RSE ratios of all samples, the variation of paleoredox condition through whole section can be achieved (Fig. 4; Table S1). In general, the Ch 7₂ and Ch 7₃ subunits show a suboxic condition with intermittent anoxic condition, and that in the Ch 7₁ subunit is dominated by suboxic to oxic condition (Fig. 4).

In addition, paleoredox chemical conditions are relevant to mineral crystallization, such as authigenic apatite and pyrite framboids (Jones and Manning, 1994; Wilkin et al., 1996). According to the formation mechanism of authigenic apatite and framboids, oxic bottom water conditions are favorable for phosphorus element preservation through the formation of authigenic apatite, and for the formation of framboids with larger mean sizes and wider size ranges (Algeo and Ingall, 2007; Wilkin et al., 1996; Yuan et al., 2017; Du et al., 2020; Wang et al., 2020). The ratio of organic carbon to phosphorus ($\text{C}_{\text{org}}:\text{P}$) in the Chang 7 unit black shale varies from 11.9 to 162.0, with an average of 85.4 (Fig. 4; Table S1). The $\text{C}_{\text{org}}:\text{P}$ fluctuation throughout the entire unit indicates

that the paleoredox condition of the Ch 7₂ and Ch 7₃ subunits is dominated by suboxic environments with intermittent anoxic environments and that the condition of the Ch 7₁ subunit is mainly in suboxic to oxic condition (Fig. 4). Based on the box-and-whisker plots of the framboid size distribution, the mean size varies from 9.7 to 16.6 μm , which indicates suboxic to oxic conditions during the deposition of the Chang 7 unit (Chen et al., 2019b). Moreover, with redox interface moving down, the decreasing “sulfurizable moieties” (such as aldehydes, alcohols, and conjugated double bonds etc.) inhibit organic matter sulfurization, then reduce the organic S:C in the sediments (Amrani and Aizenshtat, 2004; Raven et al., 2019). The sudden decline of organic S:C at the Ch 7₁ subunit suggest a more oxidized condition than the Ch 7₂ and Ch 7₃ subunits (Fig. 3).

Although the quantity-limited analysis of paleoredox chemical condition including RSEs, $\text{C}_{\text{org}}:\text{P}$ ratios, pyrite framboid morphology and organic S:C ratios are not completely unanimous for some details, the paleoredox variation tendencies of the Chang 7 unit are similar. In general, the paleoredox chemical conditions of the Ch 7₂ and Ch 7₃ subunits are dominated by suboxic condition with intermittent anoxic condition, and the Ch 7₁ subunit is mainly suboxic to oxic condition. The paleoredox condition controls the preservation of organic matter and cycles of sulfur, phosphorous and iron (Zhu et al., 2018; Liu et al., 2019a, b). In the Ch 7₁ subunit, the decreasing TOC contents and organic sulfur content, increasing P contents and change of iron speciation are respond to the alteration of paleoredox condition from suboxic to suboxic-oxic (Figs. 3 and 4).

5.3. Mechanisms inducing anomalous pyrite sulfur isotope

The abovementioned studies verify that the sulfur in the Chang 7 unit black shale comes from watermass sulfate, and the positive pyrite sulfur isotope is believed to be resulted from change of paleoredox condition (Canfield, 2001; Habicht and Canfield, 2001). However, a more sophisticated sedimentary process should be proposed to explain the formation of anomalous heavy pyrite in the Chang 7 unit black shale. In an integrated sedimentary system, sulfur cycle is usually linked with C, P, Fe cycle and trace metal elements, which are controlled by redox chemical condition (Berner, 1982; Algeo and Ingall, 2007; Cai et al., 2015). Thus, C, P, Fe speciation and Mn can be used to synergistically explain the formation mechanism of heavy pyrite.

Because the Ordos Basin is a eutrophic lake basin during the deposition of the Chang 7 unit (Chen et al., 2020), dissolved oxygen in watermass was consumed by a mount of sedimentary organic matter oxidation until exhausted, which is beneficial to microbial anaerobic respiration in sedimentary water, including denitrification, manganese reduction, iron reduction, sulfate reduction etc. in sequence (Berner, 1982; Canfield and Thamdrup, 2009; Poulton and Canfield, 2011; Lyons et al., 2014; Li et al., 2015). It should be noted that each microbial anaerobic respiration zones are not completely separate in space, and are dynamically maintained in porewater (Raiswell and Canfield, 1998; Li et al., 2015). Due to the Chang 7 unit deposited in a suboxic to oxic bottom redox condition, BSR occurred in the relative closed porewater environment under the influence of fine-grained sediments and fresh porewater with limited sulfate, which resulted in limited sulfur isotope fractionation, then to positive sulfur isotope of hydrogen sulfide (Canfield, 2001; Hurtgen et al., 2002; Huang et al., 2013). During the deposition of the Ch 7₂ and Ch 7₃ subunits of the Chang 7 unit, the paleoredox chemical condition of the bottom watermass is dominated by suboxic condition with intermittent anoxic condition, leading to microbial anaerobic respiration reacted in the porewater beneath sediment surface. The majority of oxidants such as NO_3^- , MnO_2 and FeOOH in porewater were reduced to NO_2^- , Mn^{2+} and Fe^{2+} (Canfield and Thamdrup, 2009), and the upward-diffused “heavy” H_2S reacted with active iron to form “heavy” pyrite in the Ch 7₂ and Ch 7₃ subunits (Fig. 6A; Raiswell and Canfield, 1998).

However, with the change of paleoredox condition from suboxic to

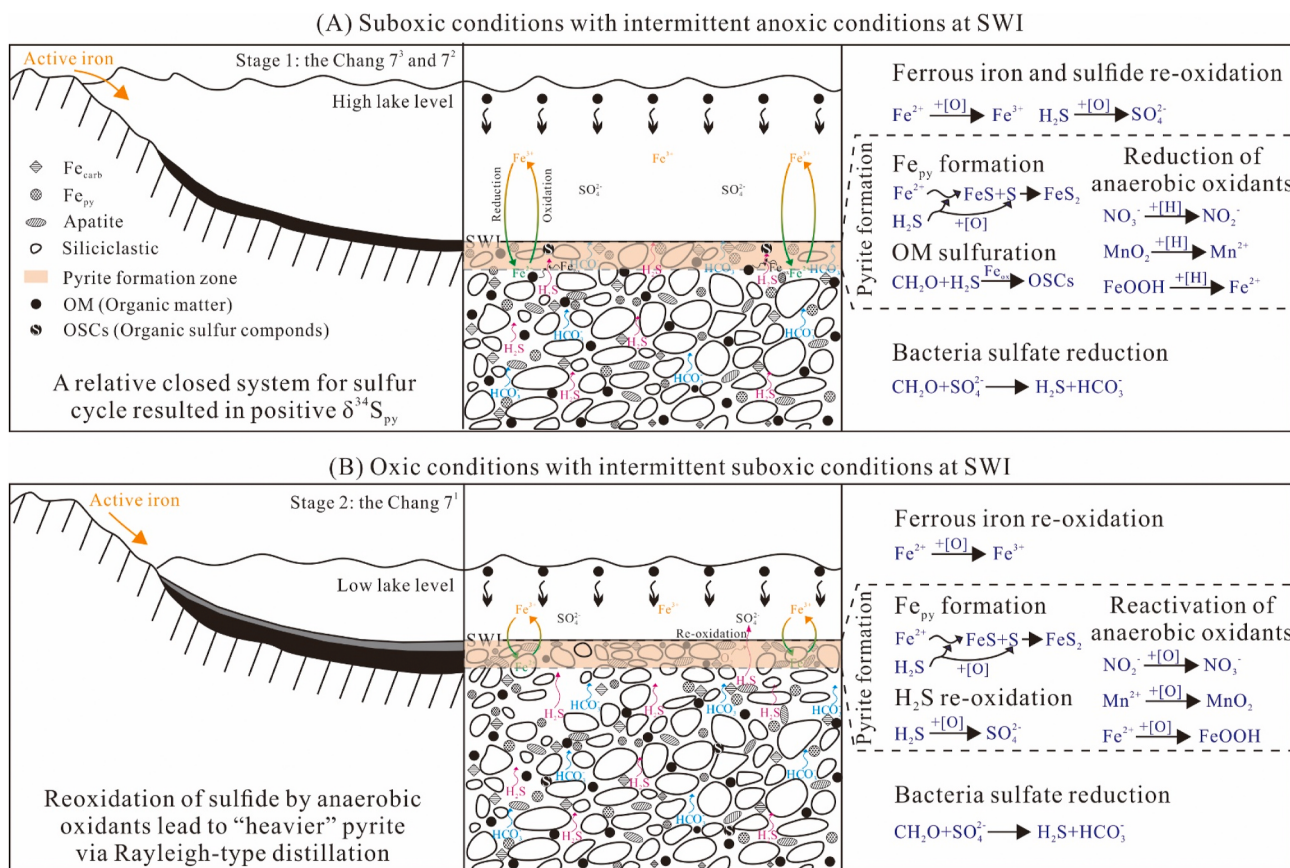


Fig. 6. The scenario of anomalous positive pyrite sulfur isotope during the deposition of the Chang 7 unit black shale. (A) The paleoredox chemical conditions were suboxic with intermittent anoxic conditions at the SWI, where limited sulfate in watermass and the overlying fine grain sediments resulted in a closed system for sulfur cycle, which led to limited sulfur isotope fractionation, then to positive pyrite sulfur isotope; (B) The paleoredox conditions change to oxic at the SWI, reoxidation of sulfide by anaerobic oxidants in porewater lead to “heavier” pyrite via Rayleigh-type distillation.

oxic during the deposition of the Ch 7₁ subunit, the redox interface moved downwards beneath the SWI, dissolved oxygen in the watermass penetrated into the sediment, which resulted in the re-oxidation of NO₂, Mn²⁺ and Fe²⁺ in the porewater (Canfield and Thamdrup, 2009). Due to the reactivation of anaerobic oxidants (NO₃⁻, MnO₂ and FeOOH etc.), most H₂S derived from BSR were reoxidation, which lead to the decrease of sulfur speciation content, and enrichment of ³⁴S in residual sulfide by 4‰–5‰ via Rayleigh-type distillation (Fig. 6B; Fry et al., 1998; Ries et al., 2009). The oxic paleoredox condition enhance the intensity of Rayleigh-type distillation and recede BSR intensity, which resulted in the negative relationship between $\delta^{13}\text{C}_{\text{org}}$ and $\delta^{34}\text{S}_{\text{py}}$ in the Ch 7₁ subunit (Fig. 6B). The decreasing pyrite and organic matter sulfur content and “heavier” pyrite formation indicated the transformation of sulfur speciation and isotopic compositions are controlled by paleoredox condition (Fig. 3). Meanwhile, the relative oxidizing environment promoted the preservation of MnO₂ and iron oxide (or hydroxide), which are consistent with the increasing content of Mn and Fe_T in the Ch 7₁ subunit (Figs. 3 and 4; Table S1). In addition, due to the Fe–P bound is the main form for P preserving in early diagenesis (Marz et al., 2008), the P contents increase with the increasing Fe_T content, which resulted in the decreasing C_{org}:P ratios in the Ch 7₁ subunit (Fig. 4).

6. Conclusions

In this study, a series of geochemical analysis performed on the lacustrine black shale in the Chang 7 unit were utilized to reconstruct the paleoredox condition, confirm the derivation of sulfur in sediments and explore the possible trigger for the anomalous positive pyrite sulfur isotope.

- (1) The positive $\delta^{34}\text{S}_{\text{py}}$ have been certified to record the sedimentary environment, and the sulfur derivation of lacustrine black shale comes from atmospheric precipitation/surface-runoff rather than hydrothermal systems.
- (2) Combined with the iron speciation analysis, organic S:C ratios, C_{org}:P ratios and size distribution of pyrite framboids in sediments, the paleoredox chemical conditions change from suboxic to oxic conditions with intermittent anoxic conditions from the bottom to top.
- (3) The limited sulfate in the watermass and the overlying fine grain sediments represent a relative closed porewater environment for sulfur cycle where microbial anaerobic respirations were resulted in limited sulfur isotope fractionation, then to positive $\delta^{34}\text{S}_{\text{py}}$.
- (4) Due to the dissolved oxygen penetrated into the sediment during the deposition of the Ch 7₁ subunit, the reactivation of anaerobic oxidants led to reoxidation of hydrogen sulfide derived from BSR, then to “heavier” pyrite via Rayleigh-type distillation.

Declaration of competing interest

The authors declare that they have no known competing financial interests or personal relationships that could have appeared to influence the work reported in this paper.

CRediT authorship contribution statement

Guo Chen: Conceptualization, Methodology, Writing - original draft. **Xiangchun Chang:** Writing - review & editing. **Wenzhe Gang:** Supervision, Funding acquisition. **Ning Wang:** Investigation. **Pengfei Zhang:**

Methodology. **Qingyun Cao:** Resources, Project administration. **Jianbin Xu:** Writing - review & editing.

Acknowledgement

This work was financially supported by the China Postdoctoral Science Foundation (Grant No.2020M672091) and the PetroChina Changqing Oilfield Company (Grant No.2016-007), and thanks them for providing samples and data assess for permission to publish this work. The authors are also grateful for the help from Ms Juan Han from Analytical Laboratory Beijing Research Institute of Uranium Geology.

Appendix A. Supplementary data

Supplementary data to this article can be found online at <https://doi.org/10.1016/j.marpetgeo.2020.104587>.

References

- Amrani, A., Aizenshtat, Z., 2004. Mechanisms of sulfur introduction chemically controlled: 634S imprint. *Org. Geochem.* 35, 1319–1336.
- Algeo, T.J., Ingall, E., 2007. Sedimentary Corg:P ratios, paleocean ventilation, and Phanerozoic atmospheric pO₂. *Palaeogeogr. Palaeoclimatol. Palaeoecol.* 256, 130–155.
- Algeo, T.J., Shen, Y.A., Zhang, T.G., Lyons, T.W., Bates, S.M., Rowe, H., Nguyen, T.K.T., 2008. Association of ³⁴S-depleted pyrite layers with negative carbonate δ¹³C excursions at the Permian/Triassic boundary: evidence for upwelling of sulfidic deep-ocean watermasses. *Geochem. Geophys. Geosyst.* 9 (4), Q04025.
- Anderson, T.F., Pratt, L.M., 1995. Isotopic evidence for the origin of organic sulfur and elemental sulfur in marine sediments. *ACS (Am. Chem. Soc.) Symp. Ser.* 612, 378–396.
- Anderson, R.F., Fleisher, M.Q., Le Huray, A.P., 1989. Concentration, oxidation state, and particulate flux of uranium in the Black Sea. *Geochem. Cosmochim. Acta* 53 (9), 2215–2224.
- Berner, R.A., 1982. Burial of organic carbon and pyrite sulfur in the modern ocean: its geochemical and environmental significance. *Am. J. Sci.* 282, 451–473.
- Berner, R.A., Raiswell, R., 1983. Burial of organic carbon and pyrite sulfur in sediments over Phanerozoic time: a new theory. *Geochem. Cosmochim. Acta* 47, 855–862.
- Bottomley, D.J., Veizer, J., Nielsen, H., Moczydlowska, M., 1992. Isotopic composition of disseminated sulfur in Precambrian sedimentary rocks. *Geochem. Cosmochim. Acta* 56, 3311–3322.
- Cai, C., Xiang, L., Yuan, Y., He, X., Chu, X., Chen, Y., Xu, C., 2015. Marine C, S and N biogeochemical process in the redox-stratified early Cambrian Yangtze ocean. *J. Geol. Soc.* 172, 390–406.
- Canfield, D.E., Raiswell, R., Westrich, J.T., Reaves, C.M., Berner, R.A., 1986. The use of chromium reduction in the analysis of reduced inorganic sulfur in sediments and shales. *Chem. Geol.* 54, 149–155.
- Canfield, D.E., 2001. Biogeochemistry of sulfur isotopes. In: Valley, J.W., Cole, D. (Eds.), *Stable Isotope Geochemistry*. Mineralogical Society of America and Geochemical Society, *Reviews of Mineralogy and Geochemistry*, vol. 43, pp. 607–636.
- Canfield, D.E., Thamdrup, B., 2009. Towards a consistent classification scheme for geochemical environments, or, why we wish the term “suboxic” would go away. *Geobiology* 7, 385–392.
- Chen, G., Gang, W.Z., Liu, Y.Z., Wang, N., Guo, Y., Zhu, C.Z., Cao, Q.Y., 2019a. High-resolution sediment accumulation rate determined by cyclostratigraphy and its impact on the organic matter abundance of the hydrocarbon source rock in the Yanchang Formation, Ordos Basin, China. *Mar. Petrol. Geol.* 103, 1–11.
- Chen, G., Gang, W.Z., Liu, Y.Z., Wang, N., Jiang, C., Sun, J.B., 2019b. Organic matter enrichment of the Late Triassic Yanchang Formation (Ordos Basin, China) under dysoxic to oxic conditions: insights from pyrite frambooid size distributions. *J. Asian Earth Sci.* 170, 106–117.
- Chen, G., Gang, W.Z., Tang, H.Z., Gao, G., Wang, N., Liu, L., Yang, S.R., Wang, Y., 2019c. Astronomical cycles and variations in sediment accumulation rate of the terrestrial lower Cretaceous Xiagou Formation from the Jiuquan Basin, NW China. *Cretac. Res.* <https://doi.org/10.1016/j.cretres.2019.06.002>.
- Chen, G., Gang, W.Z., Chang, X.C., Wang, N., Zhang, P.F., Cao, Q.Y., Xu, J.B., 2020. Paleoproductivity of the Chang 7 unit in the Ordos Basin (north China) and its controlling factors. *Palaeogeogr. Palaeoclimatol. Palaeoecol.* <https://doi.org/10.1016/j.palaeo.2020.109741>.
- Chen, D., Wang, J., Racki, G., Li, H., Wang, C., Ma, X., Whalen, M.T., 2013. Large sulphur isotopic perturbations and oceanic changes during the Frasnian–Famennian transition of the Late Devonian. *J. Geol. Soc.* 170, 465–476. <https://doi.org/10.1144/jgs2012-037>. In press.
- Chu, X.L., Zhao, R., Zang, W., Lei, J.J., Tang, Y.G., 1993. The extract and isotopic sample preparation of various sulfur compounds in coal and sedimentary rock. *Chin. Sci. Bull.* 38 (20), 1887–1890 (in Chinese with English abstract).
- Dembicki Jr., H., 2009. Three common source rock evaluation errors made by geologists during prospect or play appraisals. *AAPG (Am. Assoc. Pet. Geol.) Bull.* 93, 341–356.
- Du, W., Ji, Y., Chen, G., et al., 2020. Cyclostratigraphy and astronomical tuning during the Oligocene in the Jizhong Depression, Bohai Bay Basin, northeastern China. *Palaeogeogr. Palaeoclimatol. Palaeoecol.* 554 <https://doi.org/10.1016/j.palaeo.2020.109803>.
- Fry, B., Ruf, W., Gest, H., Hayes, J.M., 1998. Sulfur isotope effects associated with oxidation of sulfide by O₂ in aqueous solution. *Isot. Geosci.* 73, 205–210.
- Guo, H., Jia, W., Peng, P.A., Lei, Y., Luo, X., Cheng, M., Wang, X., Zhang, L., Jiang, C., 2014. The composition and its impact on the methane sorption of lacustrine shales from the Upper Triassic Yanchang Formation, Ordos Basin, China. *Mar. Petrol. Geol.* 57, 509–520.
- Habicht, K.S., Canfield, D.E., 1997. Sulfur isotope fractionation during bacterial sulfate reduction in organic-rich sediments. *Geochem. Cosmochim. Acta* 61, 5351–5361.
- Habicht, K.S., Canfield, D.E., 2001. Isotope fractionation by sulfatereducing natural populations and the isotopic composition of sulfide in marine sediments. *Geology* 29, 555–558.
- Hurtgen, M.T., Arthur, M.A., Suits, N.S., Kaufman, A.J., 2002. The sulfur isotopic composition of Neoproterozoic seawater sulfate: implications for a snowball Earth? *Earth Planet. Sci. Lett.* 203, 413–430.
- Huang, Y.J., Yang, G.S., Jian, G., et al., 2013. Marine incursion events in the late cretaceous songliao basin: constraints from sulfur geochemistry records. *Palaeogeogr. Palaeoclimatol. Palaeoecol.* 385, 152–161.
- Johnston, T.D., 2011. Multiple sulfur isotopes and the evolution of Earth's surface sulfur cycle. *Earth Sci. Rev.* 106, 161–183.
- Jones, B., Manning, D.A.C., 1994. Comparison of geochemical indices used for the interpretation of palaeoredox conditions in ancient mudstones. *Chem. Geol.* 111, 111–129.
- Kah, L.C., Lyons, T.W., Frank, T.D., 2004. Low marine sulphate and protracted oxygenation of the Proterozoic bio-sphere. *Nature* 431, 834–838.
- Kaplan, I.R., Rittenberg, S.C., 1964. Microbiological fractionation of sulphur isotopes. *J. Gen. Microbiol.* 34, 195–212.
- Kleeberg, A., 1999. Interactions between benthic phosphorus release and sulfur cycling in Lake Schärmützelsee (Germany). *Water Air Soil Pollut.* 99, 391–399.
- Li, R., Wang, Z.S., Gan, Q., Niu, X.L., Xu, W.K., 2019. Paleoenvironment conditions and organic matter accumulation in Upper Paleozoic organic-rich rocks in the east margin of the Ordos Basin, China. *Fuel* 252, 172–187.
- Li, C., Cheng, M., Algeo, T.J., Xie, S.C., 2015. A theoretical prediction of chemical zonation in early oceans (>520 Ma). *Sci. China Earth Sci.* 58, 1901–1909 (in Chinese with English abstract).
- Liu, X.T., Fike, D., Li, A.T., Dong, J., Xu, F.J., Zhuang, G.C., Rendle-Bühring, R., Wan, S. M., 2019a. Pyrite sulfur isotopes constrained by sedimentation rates: evidence from sediments on the East China Sea inner shelf since the late Pleistocene. *Chem. Geol.* 505, 66–75.
- Liu, Y.Z., Gang, W.Z., Chen, G., Sun, J.B., Jiang, C., 2018. Geochemical characteristics of aromatic hydrocarbons of Chang 7 source rocks from the Yanchi-Dingbian area, Ordos Basin. *Acta Sedimentol. Sin.* 36, 818–828.
- Liu, Q., Zhu, D., Jin, Z., Meng, Q., Li, S., 2019b. Influence of volcanic activities on redox chemistry changes linked to the enhancement of the ancient Sinian source rocks in the Yangtze craton. *Precambrian Res.* 327, 1–13.
- Lowenstein, T.K., Timofeeff, M.N., Kovalevych, V.M., Horita, J., 2005. The major-ion composition of Permian seawater. *Geochem. Cosmochim. Acta* 69, 1701–1719.
- Luo, G.M., Kump, L.R., Wang, Y.B., et al., 2010. Isotopic evidence for an anomalously low oceanic sulfate concentration following end-Permian mass extinction. *Earth Planet. Sci. Lett.* 300, 101–111.
- Lyons, T.W., Reinhard, C.T., Planavsky, N.J., 2014. The rise of oxygen in Earth's early ocean and atmosphere. *Nature* 506, 307–315.
- Lyons, T.W., Severmann, S., 2006. A critical look at iron paleoredox proxies: new insights from modern euxinic marine basins. *Geochem. Cosmochim. Acta* 70 (23), 5698–5722.
- Marz, C., Poulton, S.W., Beckmann, B., Kuster, K., Wagner, T., Kasten, S., 2008. Redox sensitivity of P cycling during marine black shale formation: dynamics of sulfidic and anoxic, non-sulfidic bottom waters. *Geochem. Cosmochim. Acta* 72, 3703–3717.
- Morford, J.L., Emerson, S., 1999. The geochemistry of redox sensitive trace metals in sediments. *Geochem. Cosmochim. Acta* 63, 1735–1750.
- Nara, F.W., Watanabe, T., Kakegawa, T., Seyama, H., Horiuchi, K., Nakamura, T., Imai, A., Kawasaki, N., Kawai, T., 2010. Climate control of sulfate influx to Lake Hovsgol, northwest Mongolia, during the last glacial–postglacial transition: constraints from sulfur geochemistry. *Palaeogeogr. Palaeoclimatol. Palaeoecol.* 298, 278–285.
- Owens, J.D., Lyons, T.W., Li, X., Macleod, K.G., Gordon, G., Kuypers, M.M.M., Anbar, A., Kuhnt, W., Severmann, S., 2012. Iron isotope and trace metal records of iron cycling in the proto-North Atlantic during the Cenomanian-Turonian oceanic anoxic event (OAE-2). *Paleoceanography* 27, PA3223.
- Pang, Y., Guo, X., Shi, B., et al., 2020. Hydrocarbon Generation Evaluation, Burial History, and Thermal Maturity of the Lower Triassic–Silurian Organic-Rich Sedimentary Rocks in the Central Uplift of the South Yellow Sea Basin, East Asia. *Energy Fuels*. <https://doi.org/10.1021/acs.energyfuels.0c00552>.
- Poulton, S.W., Canfield, D.E., 2005. Development of a sequential extraction procedure for iron: implications for iron partitioning in continental derived particulates. *Chem. Geol.* 214, 209–221.
- Poulton, S.W., Canfield, D.E., 2011. Ferruginous conditions: a dominant feature of the ocean through Earth's history. *Elements* 7, 107–112.
- Qiu, X.L., Liu, C., Mao, G., Deng, Y., Wang, F., Wang, J., 2014. Late Triassic tuff intervals in the Ordos basin, Central China: their depositional, petrographic, geochemical characteristics and regional implications. *J. Asian Earth Sci.* 80, 148–160.
- Qiu, X.W., Liu, C.Y., Mao, G.Z., Deng, Y., Wang, F.F., Wang, J.Q., 2015. Major, trace and platinum-group element geochemistry of the Upper Triassic nonmarine hot shales in the Ordos Basin, Central China. *Appl. Geochem.* 53, 42–52.

- Raiswell, R., Canfield, D.E., 1998. Sources of iron for pyrite formation in marine sediments. *Am. J. Sci.* 298, 219–245.
- Raven, M.R., Fike, D.A., Bradley, A.S., Gomes, M.L., Owens, J.D., Webb, S.A., 2019. Paired organic matter and pyrite $\delta^{34}\text{S}$ records reveal mechanisms of carbon, sulfur, and iron cycle disruption during Ocean Anoxic Event 2. *Earth Planet Sci. Lett.* 512, 27–38.
- Ries, J.B., Fike, D.A., Pratt, L.M., Lyons, T.M., Grotzinger, J.P., 2009. Superheavy pyrite ($\delta^{34}\text{S}_{\text{Py}} > \delta^{34}\text{S}_{\text{CAS}}$) in the terminal Proterozoic Nama Group, Southern Namibia: a consequence of low seawater sulfate at the dawn of animal life. *Geology* 37, 1141–1162.
- Rimmer, S.M., 2004. Geochemical paleoredox indicators in devonian-mississippian black shales, central appalachian basin (USA). *Chem. Geol.* 206, 373–391.
- Ryu, J.H., Zierenberg, R.A., Dahlgren, R.A., Gao, S.D., 2006. Sulfur biogeochemistry and isotopic fractionation in shallow groundwater and sediments of Owens Dry Lake, California. *Chem. Geol.* 229, 257–272.
- Severmann, S., McManus, J., Berelson, W.M., Hammond, D.E., 2010. The continental shelf benthic iron flux and its isotope composition. *Geochem. Cosmochim. Acta* 74 (14), 3984–4004.
- Shen, J., Feng, Q.L., Algeo, T.J., et al., 2016. Two pulses of oceanic environmental disturbance during the Permian-Triassic boundary crisis. *Earth Planet Sci. Lett.* 443, 139–152.
- Sim, M.S., Ono, S., Donovan, K., Templer, S.P., Bosak, T., 2011. Effect of electron donors on the fractionation of sulfur isotopes by a marine Desulfovibrios. *Geochem. Cosmochim. Acta* 75, 4244–4259.
- Strauss, H., Des Marais, D.J., Hayes, J.M., Summons, R.E., 1992. The carbon-isotopic record. In: Schopf, J.W., Klein, C. (Eds.), *The Proterozoic Biosphere: A Multidisciplinary Study*. Cambridge University Press, Cambridge, UK, pp. 117–127.
- Taylor, S.R., McLennan, S.M., 1995. The geochemical evolution of the continental crust. *Rev. Geophys.* 33 (2), 241–265.
- Wei, H.Y., Wei, X.M., Qiu, Z., Song, H.Y., Shi, G., 2016. Redox conditions across the G-L boundary in South China: evidence from pyrite morphology and sulfur isotopic compositions. *Chem. Geol.* 440, 1–14.
- Wang, N., Li, M., Hong, H., et al., 2019. Biological sources of sedimentary organic matter in Neoproterozoic–Lower Cambrian shales in the Sichuan Basin (SW China): Evidence from biomarkers and microfossils. *Palaeogeogr. Palaeoclimatol. Palaeoecol.* 516, 342–353. <https://doi.org/10.1016/j.palaeo.2018.12.012>.
- Wang, N., Li, M., Tian, X., et al., 2020. Climate-ocean control on the depositional watermass conditions and organic matter enrichment in Lower Cambrian black shale in the upper Yangtze Platform. *Mar. Petrol. Geol.* 120 <https://doi.org/10.1016/j.marpetgeo.2020.104570>.
- Wei, J.Y., Wang, G.Y., 1988. *Isotope Geochemistry*. Geological Publishing House, Beijing, pp. 153–165.
- Werne, J.P., Hollander, D.J., Lyons, T.W., Sinninghe-Damste, J.S., 2004. Organic sulfur biogeochemistry: recent advances and future research directions, 379. Geological Society of America, pp. 135–150.
- Wilkin, R.T., Barnes, H.L., Brantley, S.L., 1996. The size distribution of frambooidal pyrite in modern sediments: an indicator of redox conditions. *Geochem. Cosmochim. Acta* 60, 3897–3912.
- Yan, D.T., Chen, D.Z., Wang, Q.C., Wang, J.G., 2012. Predominance of stratified anoxic Yangtze Sea interrupted by short-term oxygenation during the Ordo-Silurian transition. *Chem. Geol.* 291, 69–78.
- Yang, H., Zhang, W.Z., Wu, K., Li, S.P., Peng, P.A., Qin, Y., 2010. Uranium enrichment in lacustrine oil source rocks of the Chang 7 member of the Yanchang Formation, Ordos Basin, China. *J. Asian Earth Sci.* 39, 285–293.
- Yang, J.J., 2002. *Tectonic Evolution and Oil-Gas Reservoirs Distribution in Ordos Basin*. Petroleum Industry Press, Beijing, pp. 36–37 (in Chinese).
- Yuan, W., Liu, G.D., Stebbins, A., et al., 2017. Reconstruction of redox conditions during deposition of organic-rich shales of the upper triassic Yanchang Formation, Ordos Basin, China. *Palaeogeogr. Palaeoclimatol. Palaeoecol.* 486, 158–170.
- Zaback, D.A., Pratt, L.M., Hayes, J.M., 1993. Transport and reduction of sulfate and immobilization of sulfide in marine black shales. *Geology* 21, 141–144.
- Zerkle, A.L., Kamshny Jr., A., Kump, L.R., Farquhar, J., Oduro, H., Arthur, M.A., 2010. Sulfur cycling in a stratified euxinic lake with moderately high sulfate: constraints from quadruple S isotopes. *Geochem. Cosmochim. Acta* 74, 4953–4970.
- Zhang, W.Z., Yang, H., Yang, Y.H., Kong, Q.F., Wu, K., 2008. Petrology and element geochemistry and development environment of Yanchang Formation Chang-7 high quality source rocks in Ordos Basin. *Geochimica* 37, 59–64 (in Chinese with English abstract).
- Zhang, P., Lu, S., Li, J., Chang, X., 2020. 1D and 2D Nuclear magnetic resonance (NMR) relaxation behaviors of protons in clay, kerogen and oil-bearing shale rocks. *Mar. Petrol. Geol.* 114 <https://doi.org/10.1016/j.marpetgeo.2019.104210>.
- Zhang, W.Z., Yang, H., Peng, P.A., et al., 2009. The influence of Late Triassic volcanism on the development of Chang 7 high grade hydrocarbon source rock in Ordos Basin. *Geochimica* 38 (6), 573–582 (in Chinese with English abstract).
- Zhang, W.Z., Yang, H., Xie, L.Q., Yang, Y.H., 2010. Lake-bottom hydrothermal activities and their influences on the high-quality source rock development: a case from Chang 7 source rocks in Ordos Basin. *Petrol. Explor. Dev.* 37 (4), 424–429.
- Zhang, W.Z., Yang, H., Yang, W.W., Wu, K., Liu, F., 2015. Assessment of geological characteristics of lacustrine shale oil reservoir in Chang 7 Member of Yanchang Formation. *Geochimica* 44, 505–515 (in Chinese with English abstract).
- Zhang, W.Z., Yang, H., Xie, L.Q., 2017. Controls on organic matter accumulation in the Triassic Chang 7 lacustrine shale of the Ordos Basin, central China. *Int. J. Coal Geol.* 183, 38–51.
- Zhu, D., Liu, Q., Zhou, B., Jin, Z., Li, T., 2018. Sulfur isotope of pyrite response to redox chemistry in organic matter-enriched shales and implications for components of shale gas. *Interpretation* 6 (4), 71–83.
- Zhu, X.M., Deng, X.Q., Liu, Z.L., et al., 2013. Sedimentary characteristics and model of shallow braided delta in large-scale lacustrine: an example from Triassic Yanchang Formation in Ordos Basin. *Earth Sci. Front.* 20, 19–28 (in Chinese).
- Zhu, H., Chen, K., Liu, K., He, S., 2008. A sequence stratigraphic model for reservoir sand-body distribution in the Lower Permian Shanxi Formation in the Ordos Basin, northern China. *Mar. Petrol. Geol.* 25, 731–743.
- Zou, C., Zhang, X., Luo, P., Wang, L., Luo, Z., Liu, L., 2010. Shallow-lacustrine sand-rich deltaic depositional cycles and sequence stratigraphy of the upper triassic Yanchang Formation, Ordos Basin, China. *Basin Res.* 22, 108–125.